Hindawi Publishing Corporation
EURASIP Journal on Wireless Communications and Networking
Volume 2007, Article ID 62310, 12 pages
doi:10.1155/2007/62310

*Research Article*

# Frequency Estimation in Iterative Interference Cancellation Applied to Multibeam Satellite Systems

**J. P. Millerioux,[1,2,3,4] M. L. Boucheret,[2] C. Bazile,[3] and A. Ducasse[5]**

[1] *TéSA, 14-16 Port Saint-Etienne, 31000 Toulouse, France*
[2] *Institut de Recherche en Informatique de Toulouse, Ecole Nationale Supérieure d'Electrotechnique, d'Electronique, d'Informatique, d'Hydraulique et des Télécommunications, 2 Rue Camichel, BP 7122, 31071 Toulouse, France*
[3] *Centre National d'Etudes Spatiales, 18 Avenue E. Belin, 31401 Toulouse Cedex 4, France*
[4] *Ecole Nationale Supérieure des Télécommunications, 46 Rue Barrault, 75634 Paris Cedex 13, France*
[5] *Alcatel Alenia Space, 26 Avenue J.F. Champollion, BP 1187, 31037 Toulouse, France*

Received 31 August 2006; Revised 26 February 2007; Accepted 13 May 2007

Recommended by Alessandro Vanelli-Coralli

This paper deals with interference cancellation techniques to mitigate cochannel interference on the reverse link of multibeam satellite communication systems. The considered system takes as a starting point the DVB-RCS standard with the use of convolutional coding. The considered algorithm consists of an iterative parallel interference cancellation scheme which includes estimation of beamforming coefficients. This algorithm is first derived in the case of a symbol asynchronous channel with time-invariant carrier phases. The aim of this article is then to study possible extensions of this algorithm to the case of frequency offsets affecting user terminals. The two main approaches evaluated and discussed here are based on (1) the use of block processing for estimation of beamforming coefficients in order to follow carrier phase variations and (2) the use of single-user frequency offset estimations.



## 1. INTRODUCTION

Multiuser detection appears as a promising way to mitigate cochannel interference (CCI) on the reverse link of multibeam satellite systems. It can allow considering more capacity efficient frequency reuse strategies than classical systems (in which cochannel interference is assimilated to additive noise). However, channel estimation appears to be a critical point when performed before multiuser processing. This paper proposes a multiuser detection scheme coupled with channel reestimations.

This study is the continuation of the work reported in [1]. The considered system is inspired by the DVB-RCS standard [2], with the use of convolutional coding. The algorithm is derived for a symbol-asynchronous time-invariant channel [1]. It basically consists of a parallel interference cancellation (PIC) scheme which uses hard decisions provided by single user Viterbi decoders, and includes channel reestimation. The aim of this paper is to propose results on possible adaptations of this algorithm to the more realistic case of frequency offsets affecting user terminals.

Other approaches have been proposed in the literature with similar contexts. In [3], an iterative decoding scheme is proposed with a very simplified channel model and without considerations on channel estimation issues. In [4, 5], MMSE and noniterative MMSE-SIC schemes are evaluated in a realistic context and the problem of channel estimation before multiuser processing is addressed based on pilot symbols. In this paper, we consider a joint multiuser detection and channel estimation approach, which can notably allow reducing the required number of pilot symbols, and consequently lead to more spectrally efficient transmissions, in particular for a burst access. Notice however that the algorithm considered here is suboptimal. Some potentially optimal algorithms have been studied in [1]. However, they have appeared much more complex than the one considered here, and have shown a gain in performance possibly very limited, and highly dependant on the antenna implementation.

The paper is organized as follows: the system model and assumptions are described in Section 2, Section 3 introduces the algorithm on a time-invariant channel, Section 4 is

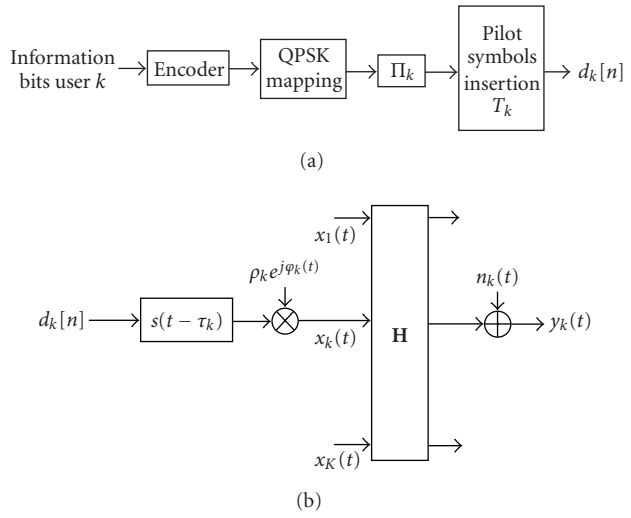


Figure 1: Transmitter and channel model.

dedicated to the study of possible adaptations with frequency offsets, and we draw conclusions in Section 5.

## 2. SYSTEM MODEL AND ASSUMPTIONS

### 2.1. Model

The considered context is the reverse link of a fixed-satellite service with a regenerative geostationary satellite, a multibeam coverage with a regular frequency reuse pattern [6], and an MF-TDMA access [2]. A "slot synchronous" system is assumed. Multiuser detection is performed onboard the satellite, after frequency demultiplexing. We choose here to work on a fictitious interference configuration characterized by carrier to interference ratios $C/I$. A more detailed presentation can be found in [1] or [7].

We consider in the following a frequency/time slot in the MF-TDMA frame. Notations are relative to complex envelops. $\cdot^*$, $\cdot^T$, $\cdot^H$, $E(\cdot)$, and $\cdot * \cdot$ denote, respectively, the conjugate, transpose, conjugate transpose, expected value, and convolution operators. Consider $K$ uplink signals associated to $K$ different cochannel cells. Under the narrowband assumption [8], we get

$$\mathbf{y}(t) = \mathbf{H}\mathbf{x}(t) + \mathbf{n}(t), \tag{1}$$

where $\mathbf{x}(t) = [x_1(t) \cdots x_K(t)]^T$ is the $K \times 1$ vector of received signals, $\mathbf{y}(t) = [y_1(t) \cdots y_K(t)]^T$ is the $K \times 1$ vector of signals at the beamformer outputs, $\mathbf{H}$ is the $K \times K$ beamforming matrix (i.e., the product of the matrix of steering vectors by the matrix of beamformer coefficients), and $\mathbf{n}(t) = [n_1(t) \cdots n_K(t)]^T$ is the vector of additive noises. Without loss of generality, we consider that the matrix $\mathbf{H}$ has its diagonal coefficients equal to 1. Additive noises are additive white Gaussian noises (AWGN) with the same variance $\sigma^2$, and are characterized by a spatial covariance matrix $\mathbf{R}_n = E(\mathbf{n}(t)\mathbf{n}(t)^H)$ which depends on the antenna implementation [1].

As regards to the waveform, the information bits are convolutionally encoded, and the coded bits are then mapped onto QPSK symbols which are interleaved differently on each beam. A burst of $N$ symbols $d_k[n]$ is composed of these interleaved symbols in which pilot symbols are inserted. We model the signals $x_k(t)$ as

$$x_k(t) = \rho_k e^{j\varphi_k(t)} \sum_{n=0}^{N-1} d_k[n] s(t - nT - \tau_k), \tag{2}$$

where $T$, $s(t)$, $\rho_k$, $\varphi_k(t)$, $\tau_k$, denote, respectively, the symbol duration, the normalized emitter filter response (square root raised cosine with rolloff equal to 0.35 [2]), the amplitude of the $k$th signal, its (possibly time-varying) carrier phase, and its time delay. The whole transmitter and channel model is summarized in Figure 1. Notice that a single frequency reference is assumed on-board the satellite.

We define the signal-to-noise ratio (SNR) for the $k$th signal as

$$\left.\frac{E_s}{N_0}\right|_k = \frac{\rho_k^2}{\sigma^2}. \tag{3}$$

Assuming an equal SNR for all users, the carrier to interference ratio for the $k$th signal can be simply defined as

$$\left.\frac{C}{I}\right|_k = \left(\sum_{l \neq k} |h_{k,l}|^2\right)^{-1}. \tag{4}$$

### 2.2. Assumptions

The algorithm is derived under the following assumptions.

(i) We assume a perfect single-user frame synchronisation and timing recovery (i.e., for the $k$th signal on the $k$th beam).
(ii) The matrix $\mathbf{H}$ is assumed time invariant on a burst duration, and unknown at the receiver.
(iii) Significant interferers are only located in adjacent cochannel cells: due to the regular reuse pattern, there are at most 6 significant interferers on a beam [6].

Let us recall that the algorithm considered in the following is suboptimal (see Section 1 and [1]): it only performs interference cancellation for the $k$th signal at the output of the $k$th beam.

## 3. ALGORITHM DESCRIPTION ON A TIME INVARIANT CHANNEL

### 3.1. Synchronous case

To simplify the presentation, we first consider a symbol-synchronous time-invariant channel, that is, $\tau_k = 0$ and $\varphi_k(t) = \varphi_k$ for all $k$. After optimal sampling, we can then consider the "one-shot" approach with

$$\mathbf{y}[n] = \mathbf{G}\mathbf{d}[n] + \mathbf{n}[n], \tag{5}$$

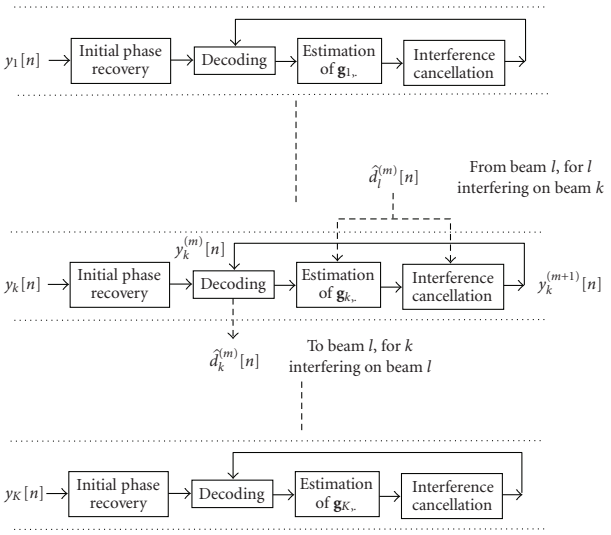


Figure 2: Block diagram of the receiver (synchronous case).

where

$$\begin{aligned}
&\mathbf{G} = \left[\mathbf{g}_1^T \cdots \mathbf{g}_K^T\right]^T = (g_{k,l}) = \mathbf{H}\,\mathrm{diag}\left(\rho_k \exp\left(j\varphi_k\right)\right),\\
&\mathbf{d}[n] = \left[d_1[n] \cdots d_K[n]\right]^T,\\
&\mathbf{y}[n] = \left[y_1[n] \cdots y_K[n]\right]^T \quad \text{with } y_k[n] = y_k(t) * s(-t)|_{t=nT},\\
&\mathbf{n}[n] = \left[n_1[n] \cdots n_K[n]\right]^T \quad \text{with } n_k[n] = n_k(t) * s(-t)|_{t=nT},\\
&E(\mathbf{n}[k]\mathbf{n}[l]) = \delta(k-l)\mathbf{R}_n.
\end{aligned} \tag{6}$$

A synoptic of the receiver is given in Figure 2, where interleaving and deinterleaving operations are omitted for simplicity. All operations are performed in parallel on the different beams, with exchange of information from one to another. The main steps are described in the following. For any parameter $c$, $\hat{c}^{(m)}$ denotes an estimate or a decision on $c$ at the $m$th iteration.

### *Channel estimation*

The channel estimation on the $k$th beam is processed by a least-square estimator using currently estimated symbols (and including pilot symbols). At the $m$th iteration, we get for the $k$th beam

$$\hat{\mathbf{g}}_k^{(m)} = \left(\sum_{n=0}^{N-1} y_k[n]\hat{\mathbf{d}}^{(m)}[n]^H\right)\left(\sum_{n=0}^{N-1} \hat{\mathbf{d}}^{(m)}[n]\hat{\mathbf{d}}^{(m)}[n]^H\right)^{-1}. \tag{7}$$

We only use for estimation (and consequently for interference cancellation in (8)) estimated symbols of the useful signal and of adjacent interfering ones (see Section 2.2. assumption (iii)), which is not specified in the equations for the sake of simplicity.

### *Interference cancellation*

The interference cancellation block output at the $m$th iteration (or the decoding block input at the $(m+1)$th iteration) is for the $n$th symbol of the $k$th user

$$y_k^{(m+1)}[n] = \hat{g}_{k,k}^{(m)*}\left(y_k[n] - \sum_{l\neq k} \hat{g}_{k,l}^{(m)}\hat{d}_l^{(m)}[n]\right). \tag{8}$$

In the case of perfect channel estimation and interfering symbol decisions, we get

$$y_k^{(m+1)}[n] = \left|g_{k,k}\right|^2 d_k[n] + g_{k,k}^* n_k[n], \tag{9}$$

interference is entirely removed, and the carrier phase is perfectly compensated.

### *Decoding*

Decoding is performed by the Viterbi algorithm, by assimilating the residual interference plus noise after deinterleaving at the decoder input to AWGN.

### *Initialization*

For the $k$th user, an initial carrier phase is estimated from pilot symbols on the $k$th beam. After phase compensation, the signal received on the $k$th beam is sent to the decoding block to initialize the iterative process.

## 3.2. Asynchronous case

We now consider a symbol-asynchronous time-invariant channel, that is, $\tau_k \neq \tau_l$ for $k \neq l$, and $\varphi_k(t) = \varphi_k$ for all $k$. We introduce

$$\begin{aligned}
u_k(t) &= \sum_{n=0}^{N-1} d_k[n]s(t - nT - \tau_k),\\
\hat{u}_k^{(m)}(t) &= \sum_{n=0}^{N-1} \hat{d}_k^{(m)}[n]s(t - nT - \tau_k),
\end{aligned} \tag{10}$$

and vectors $\mathbf{u}(t) = [u_1(t) \cdots u_K(t)]^T$ and $\hat{\mathbf{u}}^{(m)}(t) = [\hat{u}_1^{(m)}(t) \cdots \hat{u}_K^{(m)}(t)]^T$.

We get

$$\mathbf{y}(t) = \mathbf{G}\mathbf{u}(t) + \mathbf{n}(t), \tag{11}$$

where $\mathbf{G}$ is defined in Section 3.1. We refer to $\hat{u}_k^{(m)}(t)$ as the estimated $k$th signal at the $m$th iteration.

The algorithm on the asynchronous channel is then very similar to the one on the synchronous channel. For the $k$th beam, at the $m$th iteration:

(i) channel estimation is processed by a least square approach using the estimated signals at the matched filter output $\hat{\mathbf{u}}^{(m)}(t) * s(-t)$ and $y_k(t) * s(-t)$, synchronously sampled, with 2 samples per symbol (samples of $\hat{\mathbf{u}}^{(m)}(t) * s(-t)$ corresponds to $\hat{\mathbf{d}}^{(m)}[n]$ and samples of $y_k(t) * s(-t)$ corresponds to $y_k[n]$ in (7));

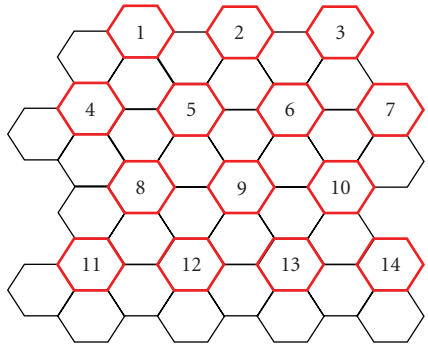


(a)

| Cell number | Number of interferers | $C/I$ [dB] |
|---|---|---|
| 1, 3 | 3 | 5 |
| 2 | 4 | 4 |
| 4, 7 | 3 | 5 |
| 5, 6 | 6 | 2 |
| 8, 10 | 5 | 3 |
| 9 | 6 | 2 |
| 11, 14 | 2 | 6 |
| 12, 13 | 4 | 4 |

(b)

Figure 3: Description of the studied configuration.

(ii) interference cancellation is processed at 1 sample per symbol, at optimal sampling instants.

More details on the implementation can be found in [1].

### 3.3. Simulation results

We use for the evaluation the fictitious configuration described in Figure 3 (which is interference configuration 2 in [1]). We consider 14 cochannel beams. The 14 users have an equal SNR. For each cell, assumption (iii) of Section 2.2 is perfectly respected, and interference is equally distributed among the interfering cells: for example we have for cell 1 $h_{1,1} = 1$, $h_{1,2} = h_{1,4} = h_{1,5} = (3 \cdot C/I|_1)^{-1/2}$, and other coefficients of the first row of $\mathbf{H}$ are set to zero. We consider the following simulation parameters.

(i) Rate 1/2 nonrecursive nonsystematic convolutional code with constraint length 7 and generators (133, 171) in octal.

(ii) Packets of 53 information bytes (ATM cell), or 430 information symbols (with closed trellis).

(iii) 32 pilot symbols, leading finally to $N = 462$ transmitted symbols in a burst.

Users timings $\tau_k$ are independent and uniformly distributed on $[0, T]$. Carrier phases $\varphi_k$ are independent and uniformly distributed on $[0, 2\pi]$. Additive noises are uncorrelated. New random interleavers and training sequences are generated at each burst.

We consider a target bit error rate (BER) equal to $2 \cdot 10^{-4}$, which is reached on AWGN channel with perfect synchronisation for $E_b/N_0$ equal to 3.2 dB. Some results for cells 5 and 6, which are symmetric, are given in Figure 4. The algorithm exhibits a degradation with respect to single-user reference of 0.15 dB after 3 iterations. At first iterations, the modulus estimate of $g_{5,9}$ and $g_{6,9}$ (which are symmetric) is widely biased: it is underestimated due to imperfect symbol decisions. As the algorithm converges, this bias is removed. In the same way, the unbiased phase estimate of $g_{5,9}$ and $g_{6,9}$ shows an error standard deviation decreasing with iterations, until it reaches the Cramer-Rao bound (CRB). This bound is more precisely the phase single-user modified CRB [9], given with our notations by

$$\mathrm{CRB}(\mathrm{Arg}(g_{k,l})) = \frac{1}{2N} |h_{k,l}|^2 \left(\frac{E_s}{N_0}\right)^{-1} [\mathrm{Rd}^2]. \quad (12)$$

Notice that these simulation results and all the following ones correspond to at least 20 packet errors and 200 binary errors for each user. Consider as an example the results at iteration 3 for $E_b/N_0 = 2.5$ dB, our evaluation of confidence intervals at 95% leads to $[4.8, 5.9] \cdot 10^{-3}$ for the BER of cell 5, $[1.2, 12.1] \cdot 10^{-3}$ for the modulus bias of coefficient $g_{5,1}$, and $[4.61, 4.89]^\circ$ for the phase error standard deviation of coefficient $g_{5,1}$.

## 4. EXTENSION TO THE CASE OF FREQUENCY OFFSETS

In geostationary systems, frequency offsets between the emitter and the receiver are mainly due to frequency instabilities of local oscillators. Considering the use of the Ka-band with low-cost user terminals, they are inevitable. In order to help the receiver to recover these frequency offsets, synchronisation bursts, which are periodically transmitted, are defined in the DVB-RCS standard. However, it always remains residual frequency offsets on the traffic bursts. In case of short bursts and low SNR, frequency and phase recovery become a challenging task, especially with a reduced number of pilot symbols.

In the following, we study possibilities of adaptation of the interference cancellation algorithm to the case of frequency deviations affecting user terminals. We first evaluate the algorithm sensitivity to frequency offsets in Section 4.1. We find that it is only suited to very low frequency offsets. We then evaluate in Section 4.2 the use of block processing for estimation of beamforming coefficients in order to cope with higher frequency offsets. As this approach is shown to lead to possible significant degradations, we finally propose and

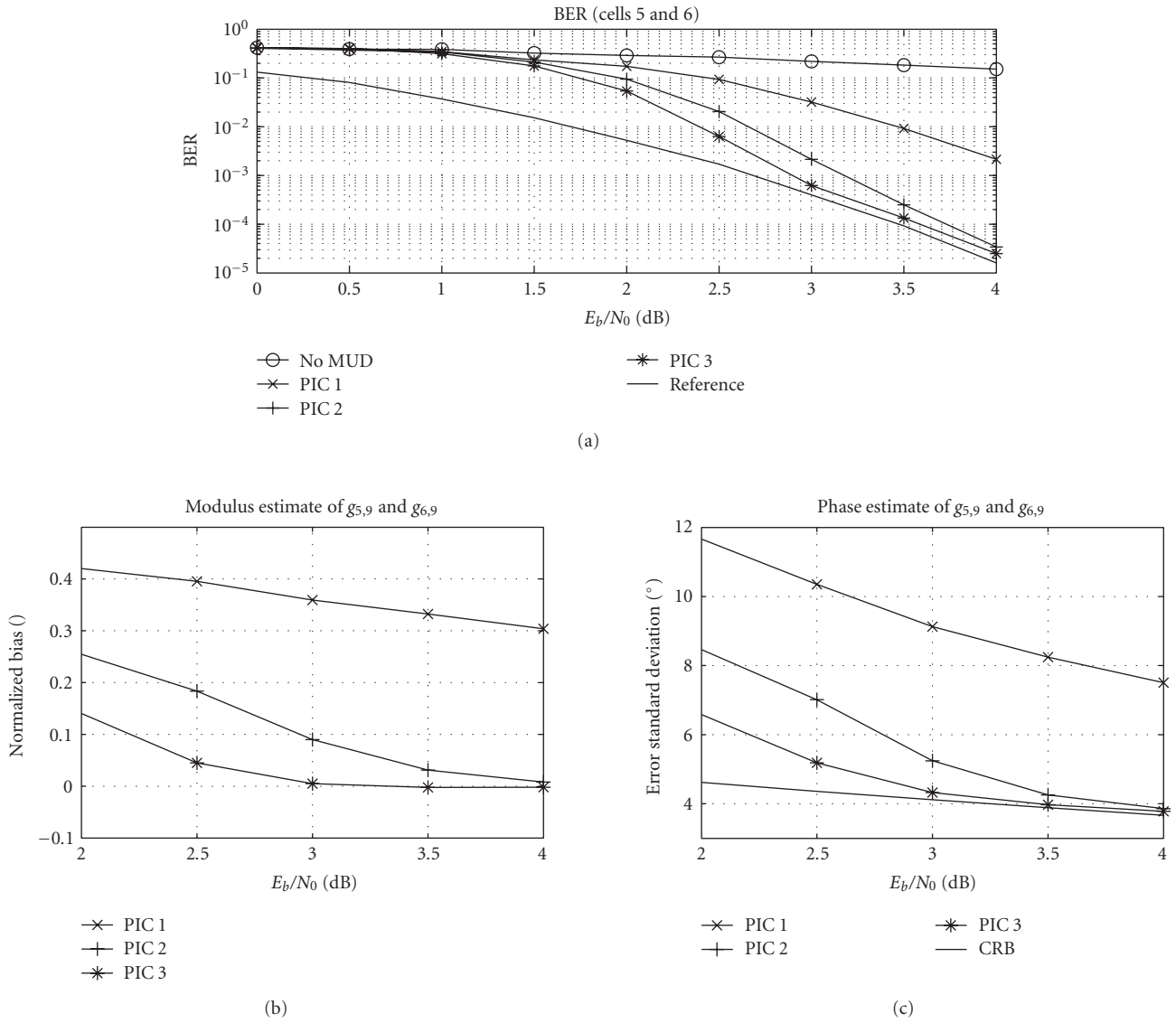


Figure 4: Results with time-invariant phases.

evaluate in Section 4.3 different schemes based on a single-user frequency estimator.

Notice the following:

(i) we possibly consider the use of pilot symbols distributed within the burst (which is not possible while strictly following the DVB-RCS standard);

(ii) all numerical values of frequency offsets are given for a burst of 462 symbols (430 information symbols and 32 pilot symbols).

### 4.1. Algorithm sensitivity to reduced frequency offsets

We evaluate in this section the algorithm sensitivity to reduced frequency offsets. As a worst case (which is the classical approach for single-user phase recovery) is difficult to define in a multiuser context, we choose here to evaluate a mean case. We model carrier phases $\varphi_k(t)$ as

$$\varphi_k(t) = \varphi_k + \Delta f_k t, \tag{13}$$

for all $k$, where the $\varphi_k$ are independent and uniformly distributed on $[0, 2\pi]$, and the $\Delta f_k T$ follow independent zero-mean Gaussian distributions with standard deviation $\sigma_{\Delta fT}$. No change is performed on the algorithm, which assumes time-invariant phases, but pilot symbols are set in the middle of the bursts (to avoid too biased initial phase estimates). Other simulation parameters are those of Section 3.3.

Some results in term of degradation with respect to single-user reference to reach the target BER are shown in Figure 5. Notice that the BER is independent of the symbol locations in the burst due to the use of interleavers. The algorithm appears maintainable with $\sigma_{\Delta fT} = 10^{-4}$, but the degradations with $\sigma_{\Delta fT} = 2 \cdot 10^{-4}$ are very large.

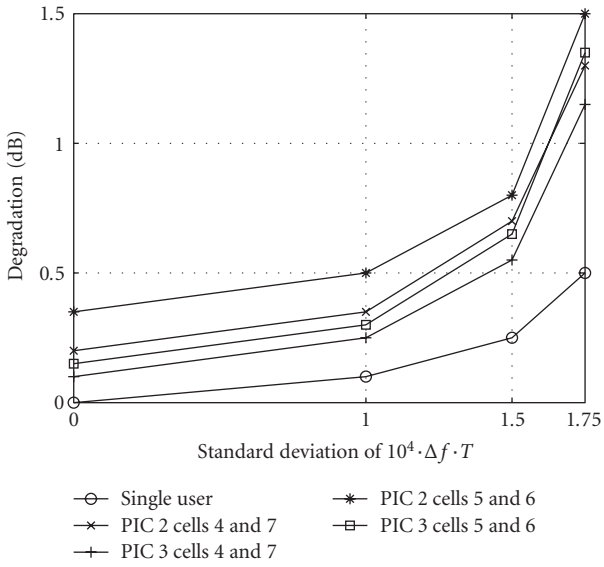


Figure 5: Degradation with frequency offsets.

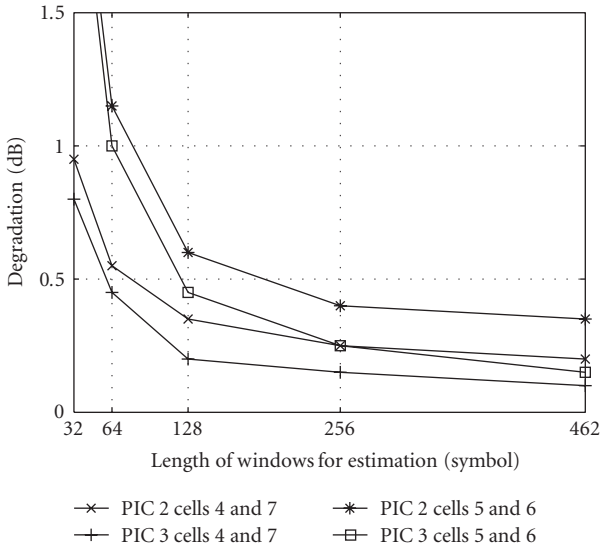


Figure 6: Degradation with reduced estimation windows.

By comparing the degradations in single-user and multiuser cases, we can see that they are similar for $\sigma_{\Delta fT} = 10^{-4}$ and for $\sigma_{\Delta fT} = 0$ (i.e., without frequency offsets). We can conclude that the degradation in the multiuser case with $\sigma_{\Delta fT} = 10^{-4}$ is mainly due to imperfect user phase recovery. Beyond $\sigma_{\Delta fT} = 10^{-4}$, it can be observed that the degradation in the multiuser case increases more quickly than the degradation in the single-user case: interference cancellation efficiency is limited. The considered algorithm is consequently limited to about $\sigma_{\Delta fT} = 10^{-4}$ for a burst length equal to 462 symbols.

### 4.2. Approach with reduced estimation windows for channel estimation

In order to cope with higher frequency offsets, we use in this section a classical block processing: the channel is no more considered invariant on the whole burst, but is considered invariant on windows of reduced length. The algorithm is modified in this way: channel estimation (7), which includes carrier phase estimations, is performed on reduced windows. Interference cancellation and phase compensation (8) is then performed on each window using the corresponding estimated coefficients $g_{k,l}$.

Channel estimation sensitivity to frequency offsets decreases when the length of estimation windows decreases, because the constellation rotations on a window are reduced. However, sensitivity to additive noise increases when the length of estimation windows decreases, because noise is averaged on shorter windows. The optimal length of estimation windows then results from a tradeoff between frequency offsets and noise.

We evaluate in this section the effect of reduced estimation windows without frequency offsets. Pilot symbols for initialization are uniformly distributed on the burst. Some results in term of degradation are shown in Figure 6. The degradation increases when the length of windows decreases. This is partially due to the fact that CRB for estimation of $g_{k,l}$ increase while the length of windows decreases, leading to a less-efficient interference cancellation and phase compensation in (8). However, the degradation is much more important for cells 5 and 6 than for cells 4 and 7, whereas the CRB for channel estimation are equal in both cases (as we have $|g_{5,2}| = |g_{5,6}| = |g_{5,9}| = |g_{5,8}| = |g_{5,4}| = |g_{5,1}| = |g_{4,1}| = |g_{4,5}| = |g_{4,8}|$). In fact, it can be seen in Figure 7 that similarly to single-user phase estimation, our channel estimator takes down from the CRB with short estimation windows and low SNR. It appears much more critical for cells 5 and 6 than for cells 4 and 7, as the least square estimation is performed on 7 (6 + 1) coefficients in the first case, and only 4 (3 + 1) in the second case. This effect also appears for longer channel estimation windows, but it is less obvious to see it.

Notice that in order to optimize the length of windows for a given $\sigma_{\Delta fT}$, we would consequently have to consider different lengths of windows for the different cells: the optimal length would be shorter for cells 4 and 7 than for cells 5 and 6.

The main conclusion is that the use of reduced estimation windows to cope with higher frequency deviations can lead to a significant loss (let us recall that evaluations have been performed in this section without frequency offsets), particularly for cells with a high number of interferers.

### 4.3. Approach with single-user frequency estimations

As the previous approach does not appear sufficient to cope with higher frequency offsets without a significant degradation, we study in this section another approach. It is based on the use of single-user frequency estimations.

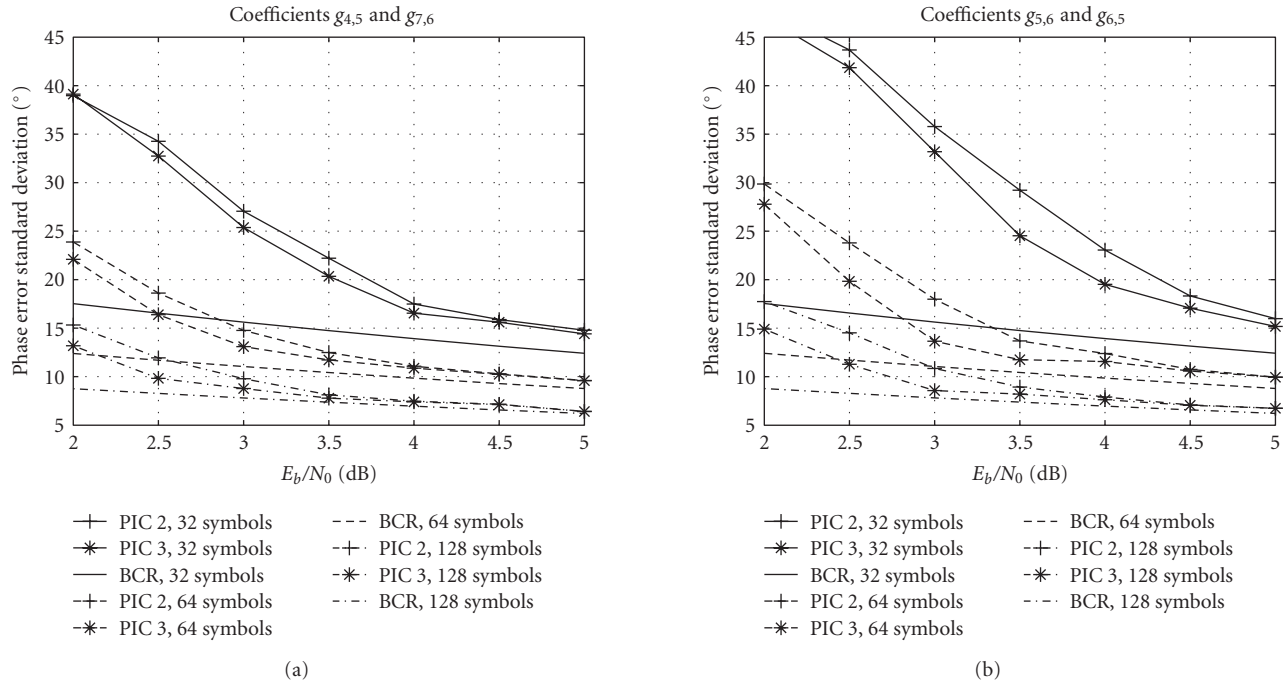


Figure 7: Channel estimation errors for different coefficients and lengths of window.

| Case | Initial PA frequency estimations | DD frequency reestimations | Reduced estimation windows for $\mathbf{g}_k$ |
|---|---|---|---|
| a | y | n | n |
| b | y | y | n |
| c up to $IT$ | n | n | y |
| c beyond $IT$ | — | y | n |

(a)

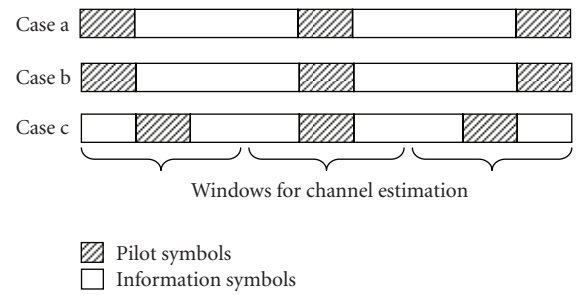


(b)

Figure 8: Approach with frequency estimations: (a) operations performed, (b) distributions of pilot symbols.

#### 4.3.1. Principle

If a frequency estimate $\Delta\hat{f}_k$ for the $k$th signal is available, it can be included in the estimated $k$th signal: $\hat{u}_k^{(m)}(t) * s(-t)$ consequently becomes $(\hat{u}_k^{(m)}(t) * s(-t))\exp(j2\pi\Delta\hat{f}_k t)$ in (7). Since the constellation rotations on the burst for $y_k(t) * s(-t)$ and $(\hat{u}_k^{(m)}(t) * s(-t))\exp(j2\pi\Delta\hat{f}_k t)$ are potentially very close (ideally identical if $\Delta\hat{f}_k = \Delta f_k$), it is then possible to keep large estimation windows to perform estimation in (7): using the whole burst allows obtaining the minimum degradation. Clearly, this approach requires "accurate" single-user frequency estimations, which become the hard task.

A first possibility is to use initial frequency estimations before interference cancellation. In this case, the estimation accuracy is limited due to the very low signal-to-interference-plus-noise ratio (unless using a very high number of pilot symbols, which decreases the spectral efficiency). Another way is to use symbol decisions for frequency estimation if it is possible to obtain sufficiently reliable symbol decisions. Many different receiver architectures can be derived. Three examples of architectures are described and evaluated in the following sections.

#### 4.3.2. Architectures with single user frequency estimations

Two modes are considered for single-user frequency estimation: the pilot aided mode (PA), based on pilot symbols, and the decision directed mode (DD), based on symbol

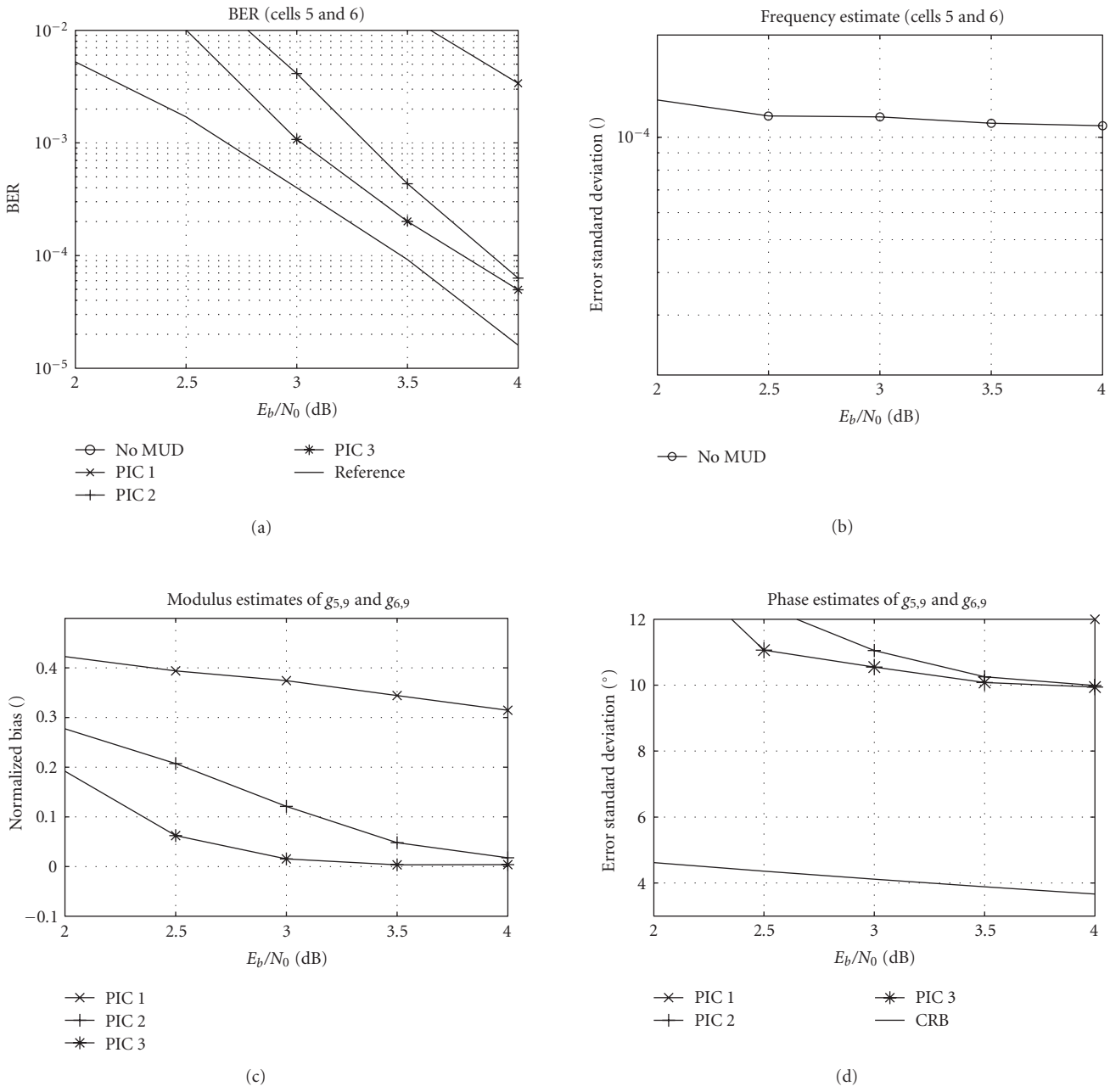


FIGURE 9: Results with frequency estimations: $\sigma_{\Delta fT} = 2 \cdot 10^{-4}$, case a.

decisions. For the PA mode, pilot symbols are distributed within the burst into 3 blocks (see Figure 8(b), cases a and b). We follow the approach of [10]. First, a mean phase is computed on each block of pilot symbols. Then, a least square estimation based on these mean phases is used to estimate the frequency. For the DD mode, the principle is the same: the burst is divided into adjacent blocks, on which mean phases are computed using symbol decisions. For the DD mode, frequency estimations are performed after interference cancellation, that is, $\Delta\widehat{f}_k^{(m)}$ are used to obtain $\widehat{\mathbf{g}}_k^{(m+1)}$.

The CRB considered for frequency estimation in DD mode is the single-user frequency modified CRB [9], given by

$$\mathrm{CRB}(\Delta f_k T) = \frac{3}{2\pi^2 N^3}\left(\frac{E_s}{N_0}\right)^{-1}. \tag{14}$$

For PA frequency estimation, the CRB is different from (14) with $N$ replaced by the number of pilot symbols (because pilot symbols are not consecutive).

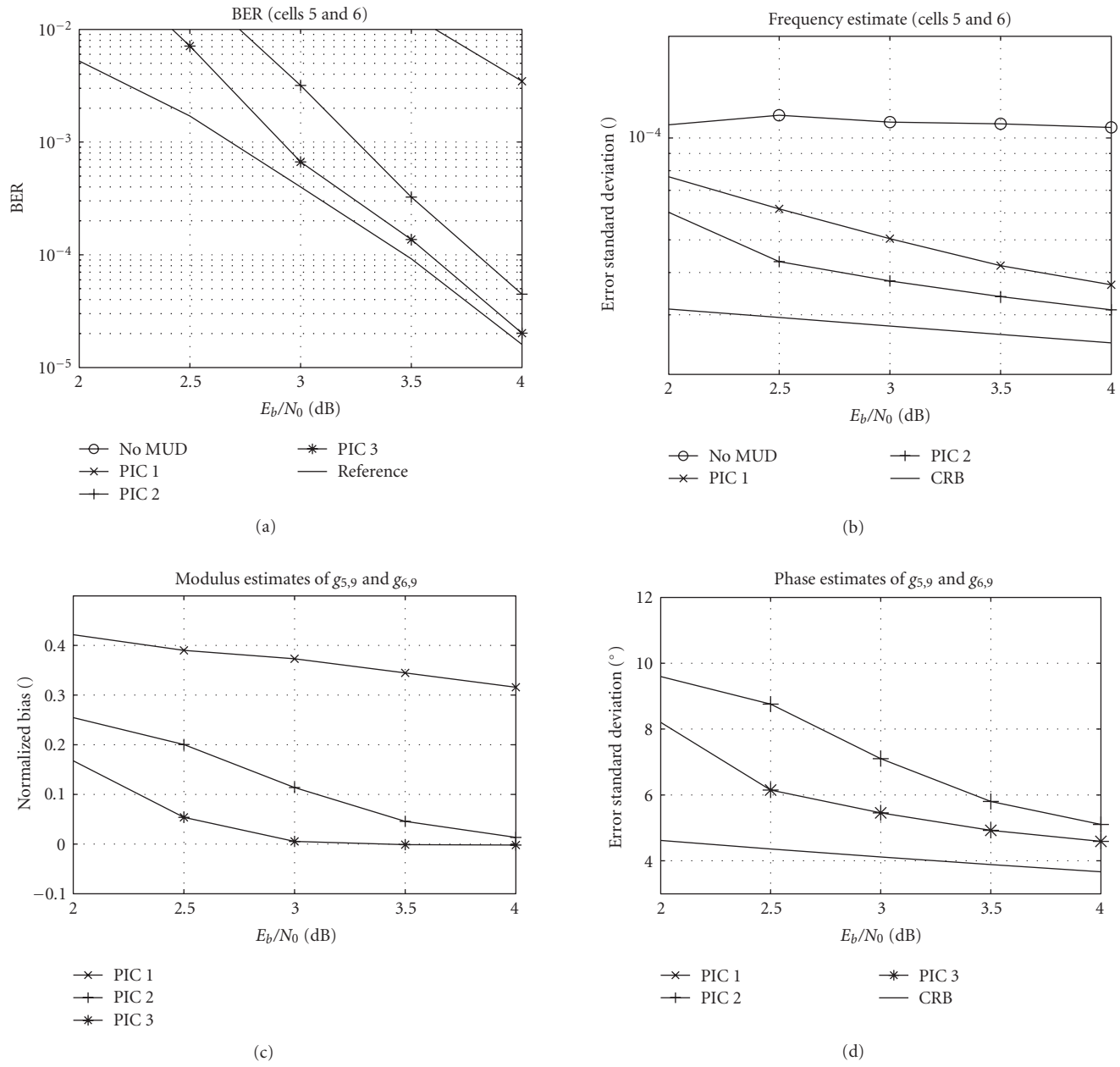


FIGURE 10: Results with frequency estimations: $\sigma_{\Delta fT} = 2 \cdot 10^{-4}$, case b.

The following three cases of receiver architecture are evaluated.

### *Case a*

PA initial frequency estimations are performed, no frequency reestimation is performed, the estimation window for the $\mathbf{g}_k$ is the whole burst.

### *Case b*

PA initial frequency estimations are performed, frequencies are reestimated in DD mode at each iteration, the estimation window for the $\mathbf{g}_k$ is the whole burst.

### *Case c*

No initial frequency estimation is performed:

(i) for iterations up to $IT$: no frequency estimation is performed, the estimation window for the $\mathbf{g}_k$ is 154 symbols for all cells (see Figure 8(b));

(ii) for iterations beyond $IT$: frequencies are reestimated in DD mode, the estimation window for the $\mathbf{g}_k$ is the whole burst.

The operations performed are summarized in Figure 8(a). In all cases, we use 32 pilot symbols. Distributions of pilot symbols are shown in Figure 8(b).

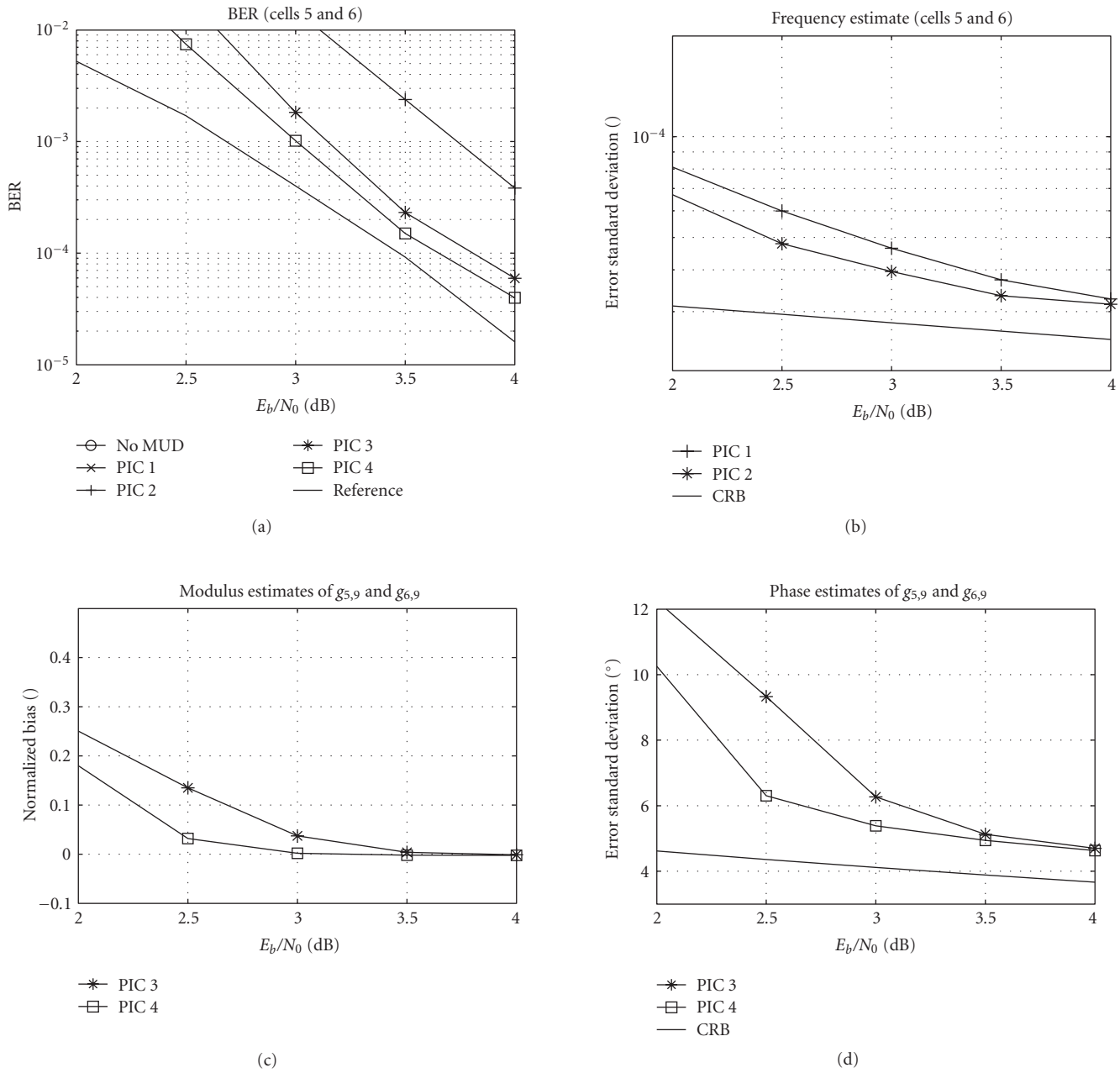


Figure 11: Results with frequency estimations: $\sigma_{\Delta fT} = 2 \cdot 10^{-4}$, case c.

#### 4.3.3. Results with $\sigma_{\Delta fT} = 2 \cdot 10^{-4}$

We first consider in this section a target $\sigma_{\Delta fT}$ equal to $2 \cdot 10^{-4}$.

Some results are given in Figures 9, 10, and 11 (with $IT = 2$) for cells 5 and 6.

In case a (Figure 9), after initial frequency estimation, the frequency error standard deviation is about $10^{-4}$. Iterative interference cancellation works, but leads to a degradation in term of BER, as in Section 4.1. The error standard deviation on the phase of $g_{5,9}$ and $g_{6,9}$ is far from the CRB, clearly because of imperfect frequency estimates.

In case b (Figure 10), DD frequency reestimations allow to get a frequency error standard deviation close to the CRB. Hence, the phase estimate error standard deviation of $g_{5,9}$ and $g_{6,9}$ is much closer to the CRB than in case a. The BER degradation is the same as that in the case without frequency offsets in Section 3.3.

In case c (Figure 11), interference cancellation is efficient but converges slower than in cases a and b. Four iterations are necessary in case c to get the BER reached with three iterations in case b.

With $\sigma_{\Delta fT} = 2 \cdot 10^{-4}$, the most efficient architecture is consequently architecture b. However, if architecture c leads

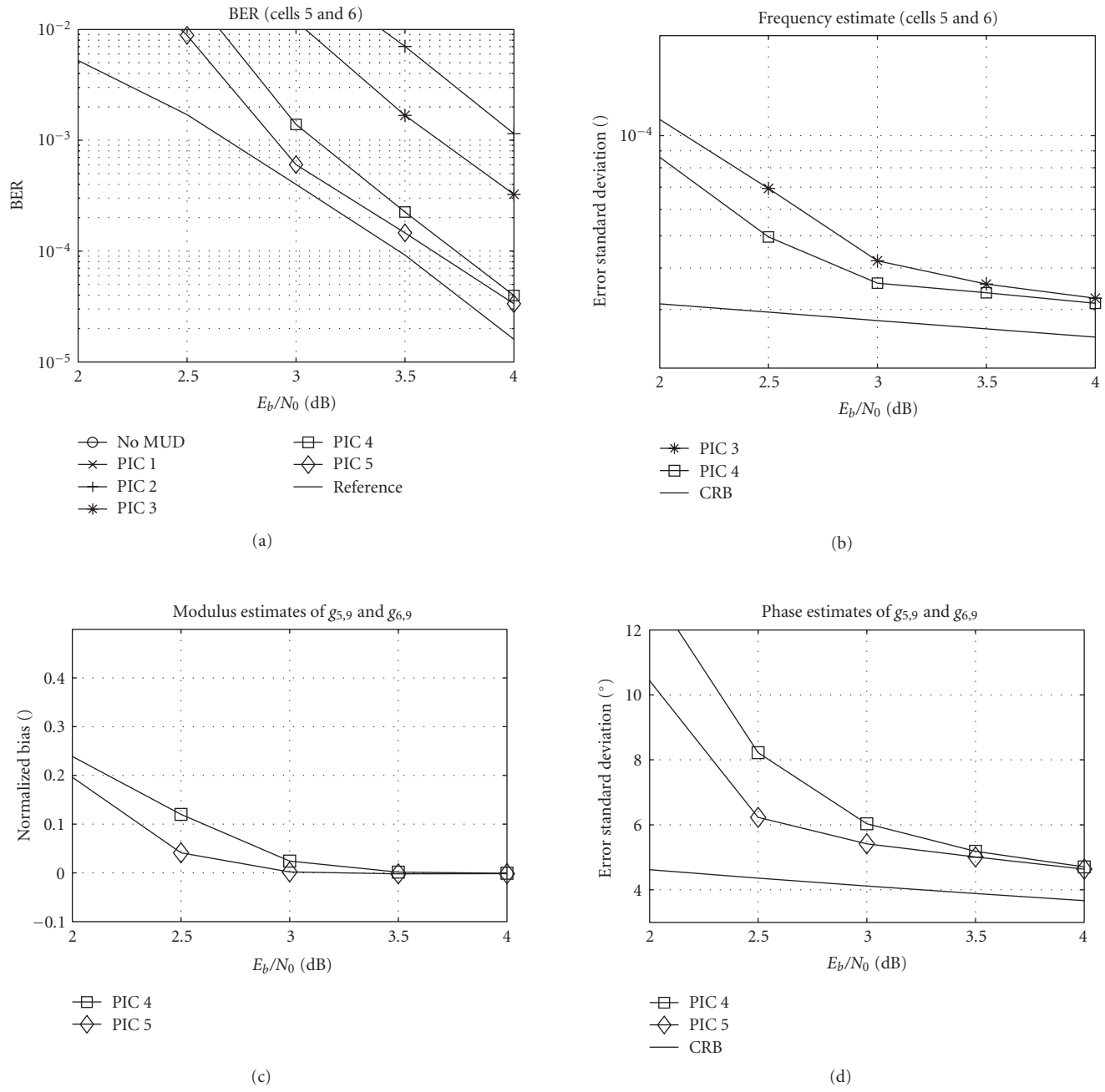


FIGURE 12: Results with frequency estimations: $\sigma_{\Delta fT} = 5 \cdot 10^{-4}$, case c.

to a slower convergence of the algorithm, a significant advantage is that it appears more suited to high-frequency offsets, as we will see in the following section.

#### 4.3.4. Results with $\sigma_{\Delta fT} = 5 \cdot 10^{-4}$

We now consider a target $\sigma_{\Delta fT}$ equal to $5 \cdot 10^{-4}$.

For this range of frequency deviations, it is very difficult to obtain reliable initial frequency estimates without a huge number of pilot symbols. On the contrary, architecture c appears to work. After optimization, we use $IT = 3$ with window lengths for $\mathbf{g}_k$ estimation from 60 to 100 symbols (depending on the number of interferers of the considered cell, Section 4.2). Some results are given in Figure 12. For $E_b/N_0$ equal to 3.2 dB, the block processing approach allows obtaining a BER equal to about $8 \cdot 10^{-3}$ at iteration 3, which is sufficient to obtain reliable frequency estimates at the following iterations. The degradation in terms of BER at iteration 5 is then similar to the case without frequency offsets.

Finally, notice that we have considered average BER along the paper. Actually, this average BER can hide some complete

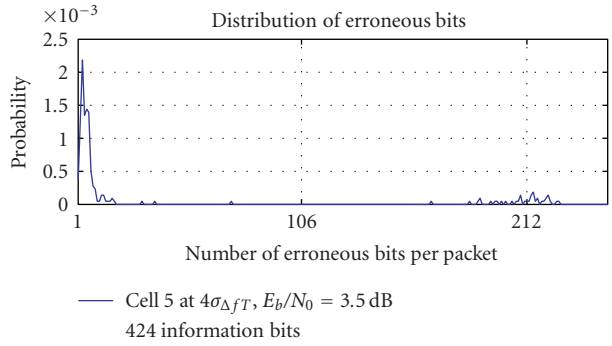


FIGURE 13: Distribution of erroneous bits: $\sigma_{\Delta fT} = 5 \cdot 10^{-4}$, iteration 5.

failures in convergence of the algorithm on some bursts, leading to a BER on these bursts much higher than the BER averaged on all bursts. These failures can result from realizations of high-frequency offsets, from cycle slip occurrences or simply from inaccurate frequency estimates. A simple approach to evaluate a probability of failure is to monitor the number of erroneous bits per burst at the algorithm output. We consider a worst case: all frequency offsets are random (Gaussian with a standard deviation $\sigma_{\Delta fT}$) except frequency offset for cell 5, which is deterministic and equal to $4\sigma_{\Delta fT} = 2 \cdot 10^{-3}$. The estimated distribution of the number of erroneous bits per burst for cell 5 at iteration 5 for $E_b/N_0$ equal to 3.5 dB is shown in Figure 13. We define a failure occurrence when the fraction of erroneous bits in a burst exceeds one fourth of the total bits in the burst ($106 = 53 \cdot 8/4$). We deduce a probability of failure equal to $2 \cdot 10^{-3}$. In the same way, with a frequency offset for cell 5 equal to $3\sigma_{\Delta fT} = 1.5 \cdot 10^{-3}$, we deduce a probability of failure equal to $10^{-4}$.

## 5. CONCLUSION

We have studied in this paper an iterative multiuser detection scheme, which includes channel estimation, suited to the reverse link of multibeam satellite communication systems. We have first derived the algorithm in the case of time invariant carrier phases. We have then discussed possible extensions to the case of frequency offsets affecting user terminals. Our main result is that if different approaches are possible for the first iterations, frequency offset estimations are necessary for final iterations in order to limit the degradation. Further works will consist in evaluations (and possibly algorithm modifications) with a more realistic channel model including phase noise.

## ACKNOWLEDGMENT

The authors would like to thank the reviewers for their thoughtful and incisive comments about this paper.

## REFERENCES

[1] J. P. Millerioux, M. L. Boucheret, C. Bazile, and A. Ducasse, "Iterative interference cancellation and channel estimation in multibeam satellite systems," *International Journal of Satellite Communications and Networking*, vol. 25, no. 3, pp. 263–283, 2007.

[2] Digital Video Broadcasting (DVB), "Interaction channel for satellite distribution systems," December 2000, ETSI EN 301 790.

[3] M. L. Moher, "Multiuser decoding for multibeam systems," *IEEE Transactions on Vehicular Technology*, vol. 49, no. 4, pp. 1226–1234, 2000.

[4] G. Caire, M. Debbah, L. Cottatellucci, et al., "Perspectives of adopting interference mitigation techniques in the context of broadband multimedia satellite systems," in *Proceedings of the 23rd AIAA International Communications Satellite Systems Conference (ICSSC '05)*, pp. 25–28, Rome, Italy, September 2005.

[5] M. Debbah, G. Gallinaro, R. Müller, R. Rinaldo, and A. Vernucci, "Interference mitigation for the reverse-link of interactive satellite networks," in *Proceedings of the 9th International Workshop on Signal Processing for Space Communications (SPSC '06)*, Noordwijk, The Netherlands, September 2006.

[6] E. Lutz, M. Werner, and A. Jahn, *Satellite Systems for Personal and Broadband Communications*, Springer, New York, NY, USA, 2000.

[7] J. P. Millerioux, "Techniques de détection multi-utilisateurs pour les communications multifaisceaux par satellite," Ph.D. dissertation, ENST, Paris, France, September 2006.

[8] L. C. Godara, "Application of antenna arrays to mobile communications—part II: beam-forming and direction-of-arrival considerations," *Proceedings of the IEEE*, vol. 85, no. 8, pp. 1195–1245, 1997.

[9] A. N. D'Andrea, U. Mengali, and R. Reggiannini, "The modified Cramer-Rao bound and its application to synchronization problems," *IEEE Transactions on Communications*, vol. 42, no. 234, pp. 1391–1399, 1994.

[10] F. Adriaensen, W. Steinert, and A. Van Doninck, "MF-TDMA burst demodulator design with pilot symbol assisted frequency estimation," in *Proceedings of the 8th ESA International Workshop on Signal Processing for Space Communications (SPSC '03)*, Catania, Italy, September 2003.